Development and validation a pyroptosis related gene prognostic index for metastatic urothelial carcinoma based on immune checkpoint blockade therapy

Jiaxing Lin
Peking University
Mengting Ding
Peking University
Caipeng Qin#
Peking University
Yuxuan Song
Peking University
Jingli Han
Peking University
Wenbo Yang
Peking University
Yiqing Du
Peking University
Tao Xu (xutao@pkuph.edu.cn)
Peking University

Research Article

Keywords: Pyroptosis, ICB, mUC, PRGPI, Prognosis

Posted Date: May 11th, 2022

DOI: https://doi.org/10.21203/rs.3.rs-1625353/v1

Abstract

Background

Immune checkpoint blockade (ICB) therapy has become a first-line treatment option for metastatic urothelial carcinoma (mUC) patients who do not meet the criteria of cisplatin. Still, only a few people can benefit from it, so useful predictive markers are needed.

Methods

Download the ICB-based mUC and chemotherapy-based bladder cancer cohorts, and extract the expression data of pyroptosis-related genes (PRG). The LASSO algorithm was used to construct the PRG prognostic index (PRGPI) in the mUC cohort, and we verified the prognostic ability of PRGPI in two mUC and two bladder cancer cohorts.

Results

Most of the PRG in the mUC cohort were immune-activated genes, and a few were immunosuppressive genes. The PRGPI composed of GZMB, IRF1, and TP63 can stratify the risk of mUC. In IMvigor210 and GSE176307 cohorts, the P-values of Kaplan Meier analysis was < 0.01 and 0.002, respectively. PRGPI could also predict ICB response, and the chi-square test of the two cohorts had P-values of 0.002 and 0.046, respectively. In addition, PRGPI can also predict the prognosis of two bladder cancer cohorts based on chemotherapy. The PRGPI and the expression of PDCD1 / CD274 had a high degree of synergistic correlation. The Low PRGPI group showed prominent characteristics of immune infiltration and was enriched in the immune signal activation pathway.

Conclusion

The PRGPI we constructed can effectively predict the treatment response and overall survival rate of mUC patients treated with ICB. The PRGPI can help mUC patients achieve individualized and accurate treatment in the future.

Introduction

Bladder cancer is the tenth most common type of cancer in the world. Urothelial cancer (UC) is the most common type of bladder cancer, accounting for 90% of bladder cancer cases in the United States and Europe (1). At the time of diagnosis, 11% of patients with bladder cancer have stage IV, accompanied by regional lymph node involvement or bone or visceral metastasis, namely metastatic urothelial carcinoma (mUC). The 5-year survival rates of regional UC and mUC vary greatly, being 34.5% and 5.2% (2), respectively. Immune checkpoint blockade (ICB) treatment has become a first-line treatment choice for

mUC patients who do not meet the conditions of cisplatin, bringing revolutionary dawn to mUC (3). However, for ICB treatment of mUC, only 20–24% of mUC patients may benefit from it, and ICB treatment has strong side effects. So far, PD-L1 expressed by tumor immune cells is the most widely studied biomarker of ICB (4). Still, the prediction accuracy of PD-L1 is relatively low due to the dynamic nature of the tumor microenvironment. TMB showed a significant correlation with the response of atezolizumab in advanced urothelial cancer (4), but it was expensive because TMB needed to be sequenced throughout the genome. Therefore, looking for new prognostic markers that can predict the ICB treatment cohort and improve the treatment response of ICB is the focus of mUC research.

Pyroptosis is a programmed cell death caused by inflammatory bodies and is dependent on caspase and GSDMs protein family. Pyroptosis cleaves GSDMs through activated caspase, causing cell membrane ruptures, which causes a robust inflammatory response (5). Immunogenic cell death (ICD) is the ability of cell death to induce an adaptive immune response. Cell death has the molecular mechanism of generating a strong inflammatory response, a form of ICD. More studies have shown that tumor clearance mediated by cell death is achieved by enhancing immune activation and function (6). It was found that in the tumor model of mice treated with intravenous NP-Gsdma3, the number of promotive cells such as CD8 + T cells and NK cells increased. In contrast, the number of inhibitory cells such as myelogenous suppressor cells and M2 macrophages decreased (7). Compared with the original T lymphocytes, the expression of GSDMD in the activated CTL of OT-1 mice was significantly increased (8). Studies have shown that GSDMB-mediated cell death acts downstream of GzmA, and CTL can transfer GzmA to GSDMB-expressing cancer cells to promote anti-tumor immunity (9). GSDME enhances anti-tumor immunity by activating cell death through GzmB as a tumor suppressor (7). pyroptosis can enhance anti-tumor immunity and is a potential marker for tumor immunotherapy.

This study downloaded transcriptome data from two mUC cohorts of ICB therapy and two chemotherapy-based bladder cancer cohorts. The immune and prognostic characteristics of the pyroptosis-related gene (PRG) were explored in the mUC cohort. The PRG prognostic index (PRGPI) was constructed using the LASSO algorithm, and the prognostic ability of PRGPI was verified in 4 cohorts. The results showed that the PRGPI could predict the treatment response and overall survival rate of the ICB treatment mUC cohort. Not only that, but PRGPI can also predict the overall survival of chemotherapy-based bladder cancer cohorts. PRGPI has a great prospect of clinical application and can be used in treatment decision-making and prognosis analysis of patients with mUC.

Materials And Methods

Data download and collation

IMvigor210 is a clinical cohort study of metastatic urothelial carcinoma (mUC) patients treated with PD-L1 drugs (atezolizumab) (10). The transcriptome and clinical data of 348 mUC patients can be obtained from the R package "IMvigor210CoreBiologies". GSE176307 is a study that uses a variety of immune checkpoint blockades (ICB) to treat mUC (11). We obtained transcriptome data of samples from this

cohort at Gene Expression Omnibus (GEO, https://www.ncbi.nlm.nih.gov/geo/) and clinical information of patients in the supplementary materials of this article. In addition, we downloaded the bladder cancer cohort (TCGA-BLCA) from The Cancer Genome Atlas (TCGA, https://portal.gdc.cancer.gov/) (12) and the GSE31684 cohort from GEO (13), all of which are bladder cancer cohorts based on chemotherapy. The transcriptome data of IMvigor210, GSE176307, and TCGA-BLCA are the second-generation sequencing data, and we uniformly convert their count format to TPM format. GSE31684 is based on the chip sequencing data of GPL570 (Affymetrix Human Genome U133 Plus 2.0 Array). Finally, we obtained four cohort transcriptome and clinical data, a total of 932 samples, including IMvigor210 (n = 348), GSE176307 (n = 88), TCGA-BLCA (n = 403), GSE31684 (n = 93).

Gene set enrichment analysis

Gene Set Enrichment Analysis (GSEA) is used to evaluate the distribution trend of genes in a predefined gene set in the gene table sorted by phenotypic correlation to determine its contribution to the phenotype (14). We download "c2.cp.kegg.v7.0.symbols" from the MSigDB database, prepare sample grouping information and gene expression matrix, and use software "GSEA_4.0.1" for GSEA analysis of the KEGG pathway. Single sample gene set enrichment analysis (ssGSEA) is a GSEA analysis for a single sample (15). We used the marker gene sets of 16 immune cells and 13 immune key pathways, and the enrichment scores of 29 immune-related gene sets were obtained by ssGSEA analysis.

Pyroptosis related gene (PRG)

Enter "pyroptosis" as the key word in the literature database, read and sort out the literature, and found a total of 52 pyroptosis pathway related genes. The expression data of PRGs were extracted from 4 cohorts of urothelial carcinoma transcriptome. 50 PRGs expression data were extracted from both IMvigor210 and GSE176307, 52 PRGs expression data were extracted from TCGA-BLCA, and 47 PRGs expression data were extracted from GSE31684.

Survival correlation analysis

Kaplan-Meier (KM) analysis is univariate survival analysis. It can be used to study the influence of one factor on survival time. We used the R packet "survival" and "survminer" for KM analysis. First, we used the function "res. cut" to calculate the best truncation value, and then grouped the samples according to the cut-off value to compare the difference in survival rate between the two groups. The p-value obtained by this method is the minimum. Receiver operating characteristic curves (ROC) is a standard used to measure the quality of classification models. The AUC value is the area covered by the ROC curve. When the AUC is greater than 0.5, it shows that the model has a certain classification ability, and the larger the AUC, the better the classification effect of the classifier. Nomogram can be used as an advanced analytical method for multi-index combined diagnosis or prediction of disease onset or progression. The graph consists of variable names, scores, and prediction probabilities in the prediction model. ROC curve and calibration curve were used to evaluate the prediction effect of the Nomogram. These processes were based on R packages "survival", "regplot", "survminer", "timeROC" and "rms".

Least Absolute Shrinkage and Selection Operator

The Least Absolute Shrinkage and Selection Operator (LASSO) is a linear regression method using L1 regularization (16). Using L1 regularization will make part of the learned feature weight 0 to achieve the purpose of sparse and feature selection. First of all, the random simulation function "glmnet" was used to build the model 1000 times. The relationship between penalty coefficient λ and gene coefficient coef was established. We can see that with the increase of λ, some gene coefficients gradually decrease to zero, indicating that the gene has little effect on the model and can eliminate the model. Then used the random simulation function "cv.glmnet" 1000 times for 10x cross-validation. The deviation value of each model can be obtained. When the deviation value is minimum, the model constructed is the best, and then the coefficient of each gene is obtained using the corresponding Lambda. Finally, a prognostic index was obtained: Risk Score = $\sum n_i (exp_i \cdot coef_i)$ (n is the number of genes, exp_i is the expression of the i gene, and $coef_i$ is the regression coefficient of the i gene).

Single cell annotation

TISCH (http://tisch.comp-genomics.org/) is a scRNA-seq database of immune microenvironments for a variety of cancers (17). TISCH can be used to query gene expression at the single-cell level to most intuitively show the content of genes in different immune cells.

Statistical analysis

The statistical analysis of this study was based on Programming Language software (Rx64 3.5.1). The heat map was drawn using the R package "pheatmap". The protein interaction network was drawn using Cytoscape_v3.6.1; the box scatter diagram was analyzed and drawn based on R packet "limma" and "ggpubr"; the violin scatter diagram was based on R packet "ggstatsplot"; and the Sankey diagram was based on R packet "ggalluvial", "ggplot2", and "dplyr". The chi-square test of the two classified variables was based on the function "ChischisqTest" of the R environment; and the pairwise comparison between groups was made by using R packets "limma" and "ggpubr".

Results

Pyroptosis-related genes are closely related to the tumor microenvironment

We explored the relationship between 50 PRGs and the immune microenvironment in the IMvigor210 cohort. First of all, we used ssGSEA to calculate the enrichment scores of 16 immune cells and 13 critical immune pathways in the transcriptome data of 348 mUC patients. The relationship heat map showed that most genes showed immune activation states, such as GZMB, GZMA, TNF, NOD2, NLRP6, NLRP3, NLRC4, IRF1, IL16, CASP5, CASP4, CASP1, and AIM2; a small number of genes showed immunosuppressive state, such as TP63 and CHMP4C (Figure 1A). GZMA and GZMB were highly positively correlated with CD8+ T cell and cytolytic activity scores, and cor > 0.8. There are four kinds of tumor therapeutic effects: PD (progressive disease), SD (stable disease), PR (partial response), and CR

(complete response). PD/SD is the ICB non-response group, PR/CR is the ICB response group. We divided the patients into two groups according to PD/SD and PR/CR and analyzed the differences. The results of thermography showed that the expression of IRF1, GZMA, GZMB, HMGB1, CYCS, CASP6, and CHMP4B increased in the PR/CR group, while the expression of GSDMC, NLRP1, NLRP3, and GPX4 decreased in the PR/CR group, which are potential markers of ICB therapy (Figure 1B). To explore the interaction network of PRG in mUC, we calculated the correlation between 50 PRG pairs and constructed a co-expression network with Cytoscape. The hub gene was found out by the MCODE algorithm, which is the pink part of the network map (Figure 1C). These genes are highly correlated with the immune-related gene set of ssGSEA. We intersected this hub and ICB differential genes to obtain GZMA, GZMB, IRF1, and NLRP3 and observed their expression differences in three immunophenotypes (desert, excluded, and inflamed). It was found that GZMB, IRF1, and NLRP3 were all low expressed in desert typing, while high expression was found in inflamed typing (Figure 1D).

Construction of pyroptosis related gene prognostic index（PRGPI）

To explore the prognostic ability of 50 genes in immunotherapy, we performed KM analysis in IMvigor210 and GSE176307 cohorts. IMvigor210 has 19 genes that can divide 348 mUC patients into high and low-risk groups (Supplementary figure 1), while GSE176307 has 14 genes that can classify 88 mUC patients into risk stratification (Supplementary figure 2). We divided the genes with prognostic ability into HR < 1 and HR > 1 for display in Figure 2A. It was found that GSDMD, GZMB, IRF1, NLRP2, NLRP7, and GZMA showed HR < 1 in both cohorts, while TP63 showed HR > 1 in both cohorts. We use the LASSO algorithm to construct the prognostic model in the IMvigor210 cohort. The prognostic model constructed by this method has the characteristics of a few variables as possible and robust stability. With the increase of lambda value, the coefficient of the gene becomes 0, which indicates that the gene has little effect on the model and can be eliminated (Figure 2B). The results of 10X cross-validation showed that when the lambda value was 3, the partial likelihood deviance of the gene was the smallest (Figure 2C). Finally, the formula of the model is as follows:

PRGPI = GZMB * (-0.00185) + IRF1* (-0.00403) + TP63 * (0.00067)

Through this formula, we can calculate the PRGPI of each patient. The best cut-off value was found by using the "res. cut" function. According to the cut-off value, the patients were divided into two groups for KM analysis, and the results were statistically significant ($p < 0.001$). The prognosis of the high-PRGPI group was significantly worse than that of the low-PRGPI group (Figure 2D). ROC curve analysis showed that the AUC values of 0.5 years, 1 year, and 1.5 years were 0.562, 0.604, and 0.597. AUC values greater than 0.5 indicate that PRGPI has a certain prognostic ability. Figure 2F is the heat map of GZMB, IRF1, TP63 expression in high-PRGPI and low-PRGPI groups. Figure 2G is the heat map of the distribution of PRGPI in patients. We used univariate cox to analyze the prognostic ability of stage, gender and PRGPI, and it was found that only PRGPI had statistical significance. PRGPI had the ability of risk stratification in TCGA_stage□, TCGA_stage□, and male of mUC. We then explored the expression of GZMB, IRF1, and TP63 in the tumor microenvironment using bladder cancer single-cell data set GSE145281. The results

showed that GZMB was significantly overexpressed in NK cells and CD8 Teff cells (Supplementary figure 3A), IRF1 was expressed in all immune cells (Supplementary figure 3B). At the same time, TP63 was not detected in all immune cells (Supplementary figure 3C).

Analysis of the relationship between PRGPI and clinical features

PRGPI is closely related to clinical factors and can guide the treatment of ICB. The Lund classification of bladder cancer can be divided into "Genomically unstable", "Basal/SCC-like", "UroA", "Infiltrated" and "UroB", and the immunophenotype is "inflamed", "excluded" and "desert". We drew the Sankey Diagram of PRGPI grouping, Lund typing, immunophenotyping, and ICB response (Figure 3A). We found an obvious enrichment trend: high-PRGPI, to UroA/Genomically unstable, to excluded/desert, to SD/PD. In PRGPI immunophenotyping, the score of desert typing was the highest, and that of inflamed typing was the lowest (Figure 3B). Infiltrated typing was the lowest in Lund typing, and UroA typing was the highest (Figure 3C). There was no difference in the expression of PRGPI between TMB $\geq$ 10 and TMB < 10. In the analysis of PRGPI and stage, the PRGPI of stage 1 was higher than that of the stage in 2 / 3 / 4. There is no relationship between PRGPI and smoking and gender (Figure 3D). We conducted a chi-square test for immunotherapy response and PRGPI in the IMvigor210 cohort. In the CR/PR group, the low-PRGPI group (35%) proportion was significantly higher than that of the high-PRGPI group (18%); in the SD/PD group, the proportion of the low-PRGPI group (65%) was significantly lower than that of the high-PRGPI (82%), with a p-value of 0.002, indicating that PRGPI can distinguish the ICB treatment response (Figure 3E). We used the ROC curve to compare the predictive ability of PRGPI, TMB, PDCD1, and CD274 for ICB treatment. The results showed that the AUC value of TMB was 0.725, PRGPI was 0.6, PDCD1 was 0.54, CD274 was 0.564 (Figure 3F). The prediction ability of PRGPI is stronger than that of PDCD1 and CD274 but weaker than that of TMB. Therefore, we combine TMB and PRGPI to predict the treatment and prognosis of ICB. It was found that 8% of SD/PD patients with TMB-H/PRGPI-L accounted for 34% of CR / PR patients, which could significantly benefit from ICB treatment (Figure 3G). The overall survival rate of the TMB-H/PRGPI-L group was significantly higher than that of other groups (Figure 3H).

PRGPI can also have a successful prognosis in GSE176307

We used the ICB treatment cohort GSE176307 to evaluate the ability to predict PRGPI. GSE176307 included 34 cases of Atezolizumab treatment, 1 case of Avelumab treatment, 2 cases of Durvalumab treatment, 5 cases of Nivolumab treatment, and 46 cases of Pembrolizumab treatment. KM analysis of PRGPI in GSE176307 showed that the prognosis of H-PRGPI was significantly worse than that of L-PRGPI (Figure 4A). The ROC curve shows that the AUC values of 0.5, 1, and 1.5 years are 0.667, 0.694, and 0.629, respectively. The results showed that PRGPI had a good ability of prognostic classification in GSE176307 (Figure 4B). Figure 4C shows the patient distribution, gene expression heat map, and survival status under PRGPI grouping. We used PRGPI to predict the progression-free survival of patients and found that PRGPI still has a good predictive ability. Both KM analysis and ROC curve show good prediction efficiency (Figure 4D-4E). The PRGPI and ICB treatment response chi-square test showed that PRGPI had a classification ability (p = 0.046, Figure 4F).

PRGPI can also predict survival in the cohort of bladder cancer dominated by chemotherapy

TCGA-BLCA and GSE31684 are two bladder cancer cohorts based on chemotherapy, containing 403 and 93 samples, respectively. The KM analysis of PRGPI in TCGA-BLCA was statistically significant (p = 0.005 and figure 5A). The results of the ROC curve show that the AUC values of 3 years, 5 years, and 7 years are all greater than 0.5. The picture on the right of Figure 5A shows the sample distribution, the heat map of gene expression, and the survival status of H-PRGPI and L-PRGPI in TCGA-BLCA. Similarly, we also verified the prognostic ability of PRGPI at GSE31684 (Figure 5B). These results suggest that PRGPI has a very generalization ability.

Construction of clinical predictive nomogram

To make it easier for doctors to make clinical decisions, we integrated the nomogram of the mUC immunotherapy cohort of the stage, gender, and PRGPI. Figure 6A is the nomogram of the IMvigor210 cohort. The calibration curve shows that the curves of 0.5, 1, and 1.5 years are all close to the middle diagonal line (Figure 6B), and the results of ROC curves show that the AUC values of 0.5, 1, and 1.5 years are 0.595, 0.606 and 0.613 (Figure 6C).

Analysis of characteristics related to PRGPI and immunity

We extracted the expression of 24 HLA molecules from the IMvigor210 cohort. The expression of most HLA molecules in H-PRGPI was lower than that in L-PRGPI, and there was significant statistical significance (Figure 7A). Then, we observed the difference between the immune cell score and the key immune gene set score between H-PRGPI and L-PRGPI. The immune score of the H-PRGPI group was generally decreased (Figure 7B-7C), indicating that the H-PRGPI group showed a state of immunosuppression. Then we explore the relationship between PDCD1, CD274, and PRGPI. The results show that PDCD1 and CD274 are overexpressed in L-PRGPI, and the correlation is more significant than 0.7 (Figure 7D-7G). Finally, we conducted a joint KM analysis of PDCD1 and PRGPI. The prognosis of patients with the H-PDCD1/L-PRGPI subgroup was the best (Figure 7H). The combined analysis of CD274 and PRGPI also showed that patients with H-CD274/L-PRGPI had a better prognosis than those in other groups (Figure 7I). We also verified these results in the GSE176307 cohort. The results of GSE176307 were very similar to those of IMvigor210 (Supplementary figure 4).

Gene set enrichment analysis

We carried out gene set analysis in IMvigor210 and GSE176307 to explore the related pathways of H-PRGPI and L-PRGPI. The results showed that only the related pathway (Figure 8A-8B) enriched to L-PRGPI was found in both cohorts. In IMvigor210, the first six pathways enriched by L-PRGPI are "ANTIGEN PROCESSING AND PRESENTATION", "AUTOIMMUNE THYROID DISEASE", "CELL ADHESION MOLECULES CAMS", "CYTOKINE-CYTOKINE RECEPTOR INTERACTION", "JAK STAT SIGNALING PATHWAY" and "NATURAL KILLER CELL MEDIATED CYTOTOXICITY". In GSE176307, the first six pathways enriched by L-PRGPI are "ANTIGEN PROCESSING AND PRESENTATION", "CELL ADHESION MOLECULES CAMS",

"CYTOKINE-CYTOKINE RECEPTOR INTERACTION", "LEISHMANIA INFECTION", "SYSTEMIC LUPUS ERYTHEMATOSUS" and "VIRAL MYOCARDITIS".

Discussion

Immune checkpoint blockade shows great potential in treating metastatic urothelial carcinoma but lack specific markers and prognostic guidance. Pyroptosis has the molecular mechanism of inducing a strong inflammatory response and plays an important role in anti-tumor immunotherapy. In this study, we used KM analysis to screen PRG with a stable prognosis, and LASSO was used to construct PRGPI. PRGPI has a certain ability to predict prognosis in two mUC cohorts based on ICB therapy. The Chi-square test showed that PRGPI had data to predict the response to immunotherapy. These results suggest that PRGPI is a potential response marker and prognostic index in the mUC cohort of ICB treatment and has important clinical significance to realize the personalized treatment of mUC.

Most of the PRGs have the characteristics of immune activation. The correlation analysis between PRG and immune enrichment score showed that most of the genes showed immune activation. Pyroptosis is mainly induced by GSDMD, involving the classical inflammatory pathway caspase-1 or non-classical pathway caspase-4/5 (6). Our study shows that CASP5, CASP4, CASP1, and GSDMD are in the state of induced immune activation. GSDMB-mediated pyroptosis is closely related to GZMA (9), while GSDME-mediated pyroptosis is related to GZMB (18). In our study, GZMA / GZMB and CD8 + T cell / cytolytic activity scores had a highly positive correlation, cor > 0.8. It is suggested that the pyroptosis mediated by bladder cancer is likely to be accomplished by the GSDMB-GZMA and GSDME-GZMB axes. In PRG, GZMB, IRF1, and NLRP3 are related to the network core and ICB treatment response and are highly expressed in the immune infiltrating type. This means GZMB, IRF1, and NLRP3 are potential markers of response to immunotherapy.

PRGPI can predict the immune response and overall survival of two ICB-treated mUC cohorts. We used the LASSO algorithm in IMvigor210 to build PRGPI. PRGPI showed good predictive ability in IMvigor210 and GSE176307, with AUC values greater than 0.55 in 0.5 / 1 /1.5 years. In previous studies, many bladder cancers have been constructed, but few studies have been specifically used to predict mUC cohorts based on ICB therapy. The Siteng study used IMvigor210 to build a prognostic model for the mUC cohort but did not use another cohort for verification (19). Our constructed PRGPI has a robust prognostic ability in both IMvigor210 and GSE176307. Some pyroptosis-related prognostic models for bladder cancer have been constructed (20, 21). Still, these models are used to analyze the prognosis of bladder cancer cohorts dominated by chemotherapy. Still, they do not have the same predictive effect for mUC cohorts of ICB treatment. This study is the first to use two cohorts to validate the mUC cohort based on ICB therapy, which has important clinical application value. The Chi-square test showed that PRGPI could predict the response to ICB treatment in IMvigor210 ($p = 0.002$). The low PRGPI group showed a higher proportion of PR/CR, while the high PRGPI group showed the opposite. In GSE176307, it shows a certain prediction effect, $p = 0.046$. These results demonstrate the great potential of PRGPI in predicting the therapeutic response of ICB and provide a new strategy for individualized treatment of mUC.

PRGPI can predict the cohort of bladder cancer treatment based on chemotherapy. In the past 30 years, the treatment of mUC has been based on platinum. Therefore, we downloaded the chemotherapy-based bladder cancer cohort TCGA-BLCA and GSE31684 and used PRGPI to predict the overall survival rate. The AUC values of 3 / 5 / 7 years were greater than 0.5, and KM analysis had significant statistical significance. PRGPI has predictive ability in four cohorts with a sample size of 932, so it has broad applicability and robustness.

Low PRGPI group has the characteristics of immune activation. The results of the Sankey diagram showed that patients with low-PRGPI, basal/SCC-like, and inflamed characteristics showed an excellent immune response to ICB treatment. In the study of Lund typing (22), basal/SCC-like represents the subtype with the worst prognosis, while this study shows that patients with a class of basal/SCC-like can reverse the prognosis by immunotherapy. The scores of CD8 + T cell and cytolytic activity increased significantly in low PRGPI, which indicated that low PRGPI had a better response to ICB, which may be caused by the enhanced killing ability of CD8 + T cell. The correlation between PRGPI and PDCD1 / CD274 was greater than 0. 7. It shows that PRGPI has a strong synergistic effect with PDCD1 and CD274. We know that CD274 is the most widely studied marker of ICB. However, because CD274 can be expressed in both tumor cells and immune cells, with intra-tumor heterogeneity (23) and differential expression between metastatic and primary lesions (24), the stability of the detected CD274 is poor. When the patients with mUC were in the state of low PRGPI and low CD274, the prognosis was significantly better than that of other groups. It is suggested that PRGPI can be combined with CD274 to analyze the prognosis of mUC cohort.

Although the PRGPI we constructed shows robust prediction ability, it also has some limitations. This study is based on published data sets, which need to be further verified by our own hospital cohort in the future; there are no further experimental studies on the genes of the model in vivo and in vitro; the IMvigor210 cohort are treated with Atezolizumab, and the GSE176307 cohort is treated with a variety of ICBs, so the model needs to be further optimized in the future to build prognostic markers suitable for specific ICB treatment.

Conclusion

We constructed the prognostic index of pyroptosis-related genes in metastatic urothelial cancer treated with immune checkpoint blockades. This index can predict immune response and overall survival rate in two mUC cohorts, and help mUC patients achieve individualized and accurate treatment.

Declarations

Funding

This work was supported by National Key Research and Development Program of China (no. 2018YFA0902802), Natural science foundation of Beijing, China(no. 7202219), National natural science

foundation of China (no. 81802533), Beijing Municipal Science & Technology Commission (no. Z191100006619010).

Competing Interests

The authors have no relevant financial or non-financial interests to disclose.

Author Contributions

Jiaxing Lin, Mingting Ding, and Caipeng Qin conducted data analysis and written manuscripts; Yuxuan Song, Jingli Han, and Wenbo Yang assisted in drawing pictures and collecting data; Yiqing Du and Tao Xu provided ideas and designed experiments.

Data Availability

There is no new data produced by this research.

Ethics approval

Not applicable.

Consent to publish

Not applicable

References

1. Heath Ei, Rosenberg Je. The biology and rationale of targeting nectin-4 in urothelial carcinoma. Nature reviews Urology (2021) 18(2):93–103. doi: 10.1038/s41585-020-00394-5. PubMed PMID: 33239713.
2. Siefker-Radtke A, Curti B. Immunotherapy in metastatic urothelial carcinoma: focus on immune checkpoint inhibition. Nature reviews Urology (2018) 15(2):112–24. doi: 10.1038/nrurol.2017.190. PubMed PMID: 29205200.
3. Bellmunt J, De Wit R, Vaughn Dj, Fradet Y, Lee Jl, Fong L, et al. Pembrolizumab as Second-Line Therapy for Advanced Urothelial Carcinoma. The New England journal of medicine (2017) 376(11):1015–26. doi: 10.1056/NEJMoa1613683. PubMed PMID: 28212060.
4. Rosenberg Je, Hoffman-Censits J, Powles T, Van Der Heijden Ms, Balar Av, Necchi A, et al. Atezolizumab in patients with locally advanced and metastatic urothelial carcinoma who have progressed following treatment with platinum-based chemotherapy: a single-arm, multicentre, phase 2 trial. Lancet (London, England) (2016) 387(10031):1909–20. doi: 10.1016/s0140-6736(16)00561-4. PubMed PMID: 26952546.
5. Liu X, Xia S, Zhang Z, Wu H, Lieberman J. Channelling inflammation: gasdermins in physiology and disease. *Nat Rev Drug Discov* (2021) 20(5):384–405. doi: 10.1038/s41573-021-00154-z. PubMed

PMID: 33692549.

6. Loveless R, Bloomquist R, Teng Y. Pyroptosis at the forefront of anticancer immunity. Journal of experimental & clinical cancer research: CR (2021) 40(1):264. doi: 10.1186/s13046-021-02065-8. PubMed PMID: 34429144.
7. Wang Q, Wang Y, Ding J, Wang C, Zhou X, Gao W, et al. A bioorthogonal system reveals antitumour immune function of pyroptosis. Nature (2020) 579(7799):421–6. doi: 10.1038/s41586-020-2079-1. PubMed PMID: 32188939.
8. Xi G, Gao J, Wan B, Zhan P, Xu W, Lv T, et al. GSDMD is required for effector CD8 T cell responses to lung cancer cells. Int Immunopharmacol (2019) 74:105713. doi: 10.1016/j.intimp.2019.105713. PubMed PMID: 31276977.
9. Zhou Z, He H, Wang K, Shi X, Wang Y, Su Y, et al. Granzyme A from cytotoxic lymphocytes cleaves GSDMB to trigger pyroptosis in target cells. Science (2020) 368(6494). doi: 10.1126/science.aaz7548. PubMed PMID: 32299851.
10. Mariathasan S, Turley Sj, Nickles D, Castiglioni A, Yuen K, Wang Y, et al. TGFβ attenuates tumour response to PD-L1 blockade by contributing to exclusion of T cells. Nature (2018) 554(7693):544–8. doi: 10.1038/nature25501. PubMed PMID: 29443960.
11. Rose Tl, Weir Wh, Mayhew Gm, Shibata Y, Eulitt P, Uronis Jm, et al. Fibroblast growth factor receptor 3 alterations and response to immune checkpoint inhibition in metastatic urothelial cancer: a real world experience. Br J Cancer (2021). doi: 10.1038/s41416-021-01488-6. PubMed PMID: 34294892.
12. Robertson Ag, Kim J, Al-Ahmadie H, Bellmunt J, Guo G, Cherniack Ad, et al. Comprehensive Molecular Characterization of Muscle-Invasive Bladder Cancer. Cell (2017) 171(3):540 – 56.e25. doi: 10.1016/j.cell.2017.09.007. PubMed PMID: 28988769.
13. Riester M, Werner L, Bellmunt J, Selvarajah S, Guancial Ea, Weir Ba, et al. Integrative analysis of 1q23.3 copy-number gain in metastatic urothelial carcinoma. Clinical cancer research: an official journal of the American Association for Cancer Research (2014) 20(7):1873–83. doi: 10.1158/1078-0432.ccr-13-0759. PubMed PMID: 24486590.
14. Mootha Vk, Lindgren Cm, Eriksson Kf, Subramanian A, Sihag S, Lehar J, et al. PGC-1alpha-responsive genes involved in oxidative phosphorylation are coordinately downregulated in human diabetes. Nat Genet (2003) 34(3):267–73. doi: 10.1038/ng1180. PubMed PMID: 12808457.
15. Barbie Da, Tamayo P, Boehm Js, Kim Sy, Moody Se, Dunn If, et al. Systematic RNA interference reveals that oncogenic KRAS-driven cancers require TBK1. Nature (2009) 462(7269):108–12. doi: 10.1038/nature08460. PubMed PMID: 19847166.
16. Friedman J, Hastie T, Tibshirani R. Regularization Paths for Generalized Linear Models via Coordinate Descent. Journal of statistical software (2010) 33(1):1–22. PubMed PMID: 20808728.
17. Sun D, Wang J, Han Y, Dong X, Ge J, Zheng R, et al. TISCH: a comprehensive web resource enabling interactive single-cell transcriptome visualization of tumor microenvironment. Nucleic Acids Res (2021) 49:D1420-D30. doi: 10.1093/nar/gkaa1020. PubMed PMID: 33179754.

18. Zhang Z, Zhang Y, Xia S, Kong Q, Li S, Liu X, et al. Gasdermin E suppresses tumour growth by activating anti-tumour immunity. Nature (2020) 579(7799):415–20. doi: 10.1038/s41586-020-2071-9. PubMed PMID: 32188940.
19. Chen S, Zhang N, Wang T, Zhang E, Wang X, Zheng J. Biomarkers of the Response to Immune Checkpoint Inhibitors in Metastatic Urothelial Carcinoma. *Frontiers in immunology* (2020) 11:1900. doi: 10.3389/fimmu.2020.01900. PubMed PMID: 32983112.
20. Fu J, Wang Y. Identification of a novel pyroptosis-related gene signature for predicting prognosis in bladder cancer. Cancer Invest (2021):1–24. doi: 10.1080/07357907.2021.1991944. PubMed PMID: 34644219.
21. Chen X, Chen H, Yao H, Zhao K, Zhang Y, He D, et al. Turning up the heat on non-immunoreactive tumors: pyroptosis influences the tumor immune microenvironment in bladder cancer. Oncogene (2021). doi: 10.1038/s41388-021-02024-9. PubMed PMID: 34588621.
22. Sjödahl G, Lauss M, Lövgren K, Chebil G, Gudjonsson S, Veerla S, et al. A molecular taxonomy for urothelial carcinoma. *Clinical cancer research: an official journal of the American Association for Cancer Research* (2012) 18(12):3377-86. doi: 10.1158/1078-0432.ccr-12-0077-t. PubMed PMID: 22553347.
23. Mclaughlin J, Han G, Schalper Ka, Carvajal-Hausdorf D, Pelekanou V, Rehman J, et al. Quantitative Assessment of the Heterogeneity of PD-L1 Expression in Non-Small-Cell Lung Cancer. JAMA oncology (2016) 2(1):46–54. doi: 10.1001/jamaoncol.2015.3638. PubMed PMID: 26562159.
24. Callea M, Albiges L, Gupta M, Cheng Sc, Genega Em, Fay Ap, et al. Differential Expression of PD-L1 between Primary and Metastatic Sites in Clear-Cell Renal Cell Carcinoma. Cancer immunology research (2015) 3(10):1158–64. doi: 10.1158/2326-6066.cir-15-0043. PubMed PMID: 26014095.

Figures

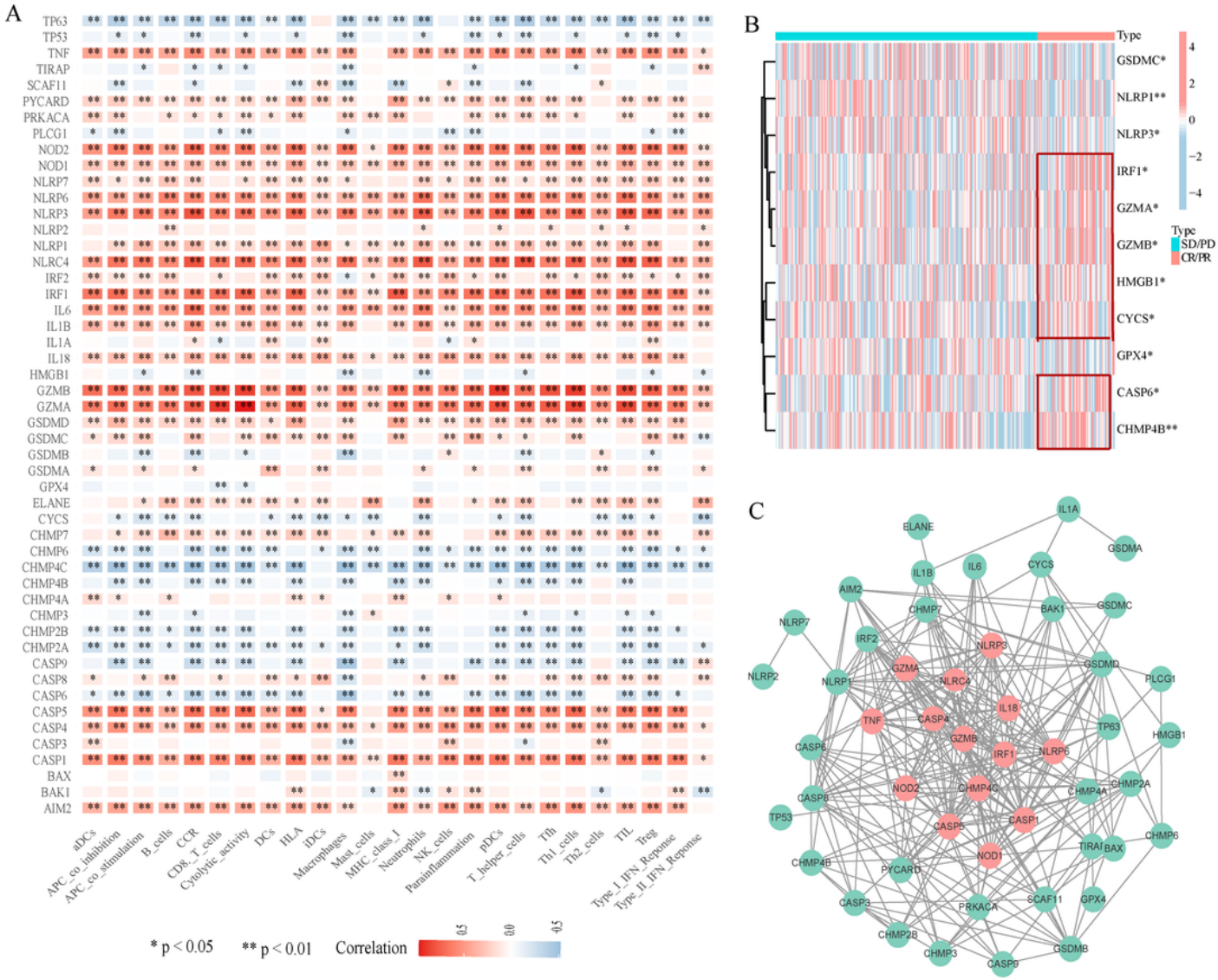

Figure 1

Immune microenvironment analysis of PRG. (A) The correlation heat map of 50 PRG and ssGSEA immune score. (B) The difference of PRG between the ICB response group and the non-response group. (C) The co-expression network of PRG. (D) Differential expression of GZMA, GZMB, IRF1, and NLRP3Z in three immunophenotypes.

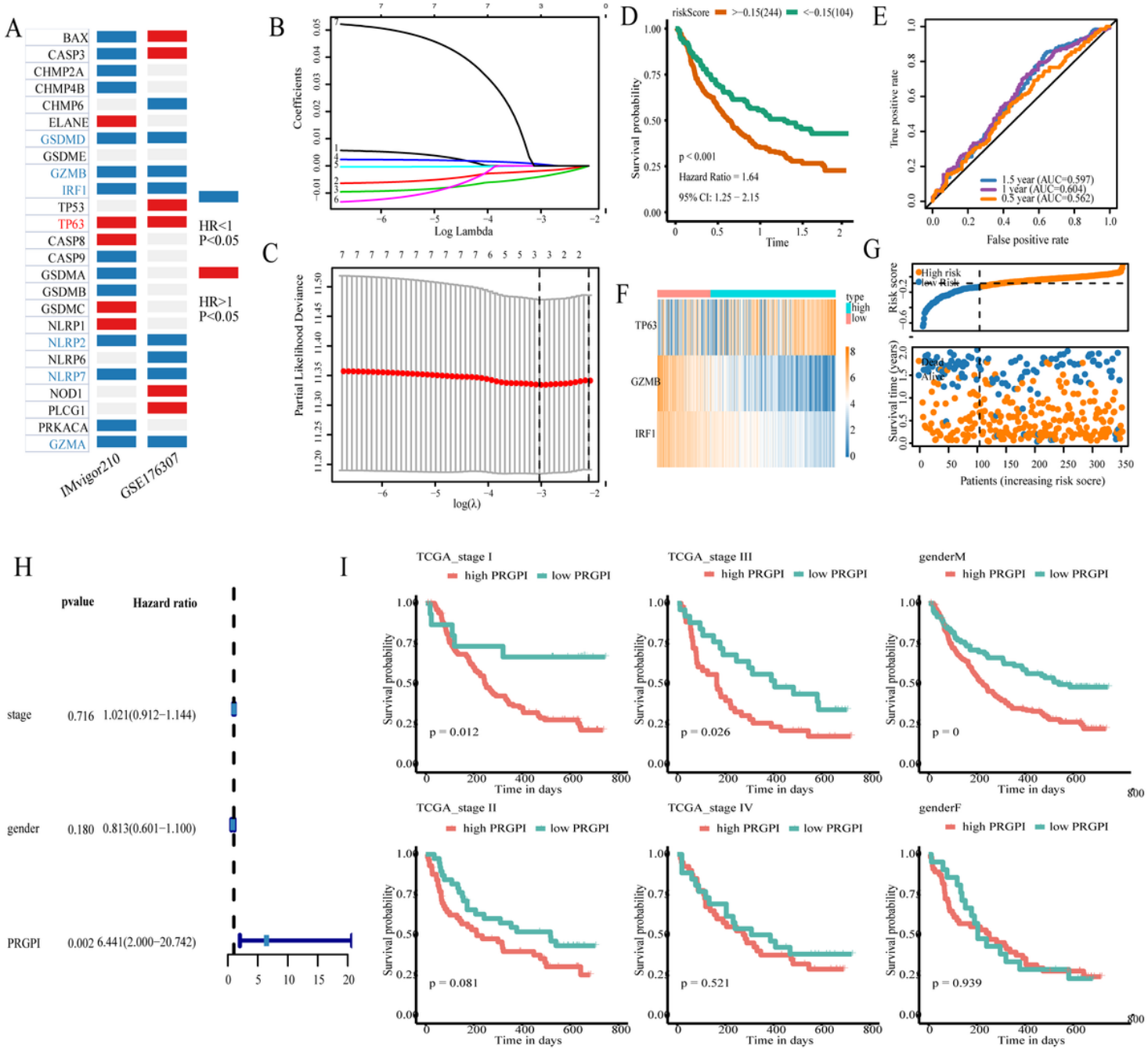

Figure 2

Build the PRGPI in the IMvigor210 cohort. (A) KM analysis results for IMvigor210 and GSE176307 cohorts. (B) The graph of the relationship between Gene coefficient and Lambda. (C)The result of 10X cross-validation. (D) KM analysis of PRGPI in the IMvigor210 cohort. (E) ROC curve analysis of PRGPI. (F) Gene expression heat map of GZMB, IRF1, and TP63. (G) The distribution heat map of PRGPI in patients. (H) Univariate cox analysis of PRGPI, gender, and stage. (I) KM analysis of PRGPI in different clinical subgroups.

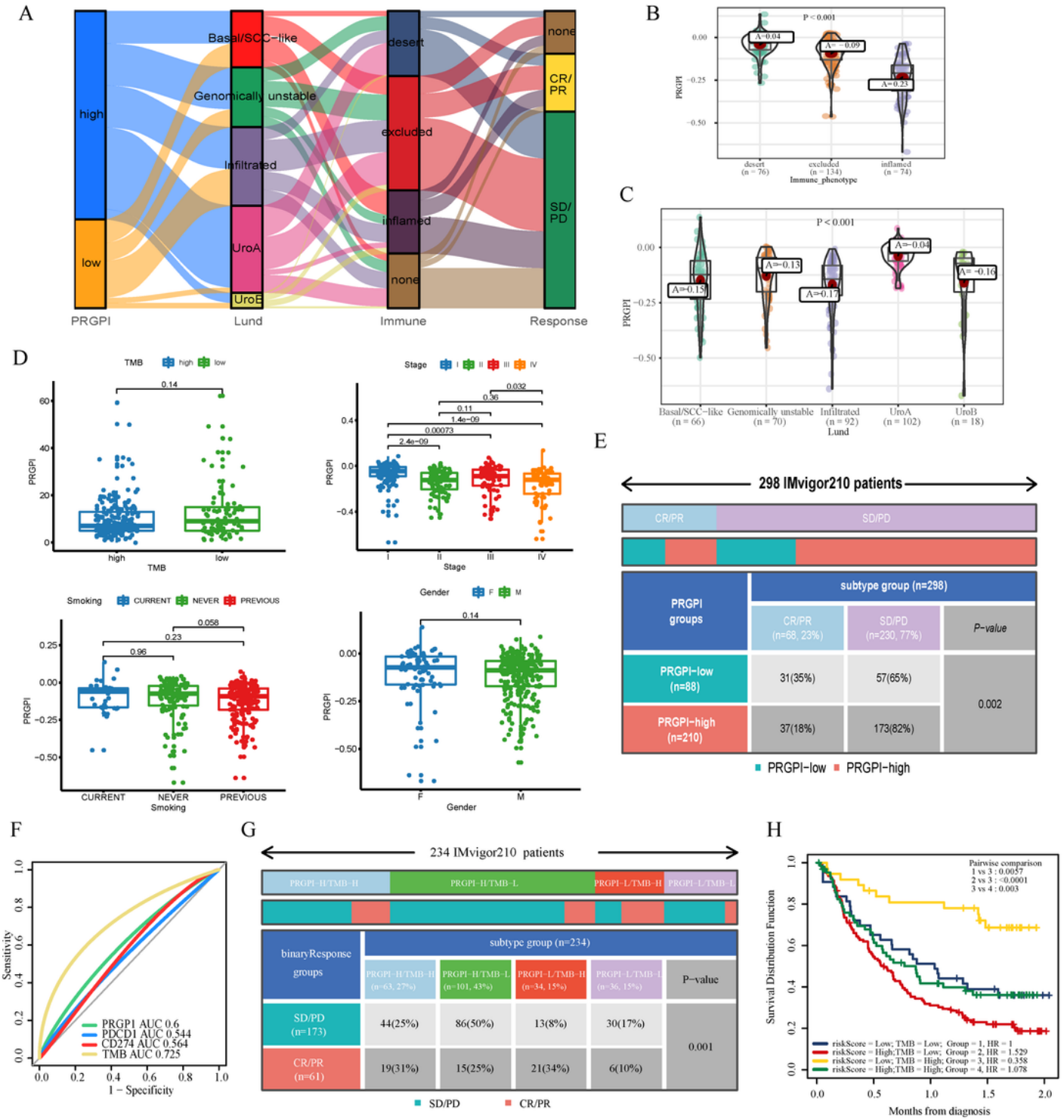

Figure 3

Analysis of the relationship between PRGPI and clinical factors. (A) Sankey Diagram of multiple clinical types of IMvigor210. (B) Immune subtype and PRGPI's violin scatter diagram. (C) Lund typing and PRGPI's violin scatter chart. (D) Box scatter diagrams of TMB, stage, smoking, and gender with PRGPI. (E) Chi-square test for PRGPI and ICB reactions. (F) The ROC curve evaluated the ability of multiple factors to classify the response to ICB treatment. (G) Chi-square test of the prediction of ICB treatment response by

TMB and PRGPI combined grouping. (H) TMB and PRGPI were used to analyze the prognosis of the IMvigor210 cohort.

Figure 4

Using GSE176307 to validate PRGPI. (A) The KM analysis curve of PRGPI to predict the overall survival rate. (B). ROC curve. (C) PRGPI distribution map. (D) KM analysis curve of PRGPI predicting disease-free survival. (E) Chi-square test of PRGPI and immunotherapy response.

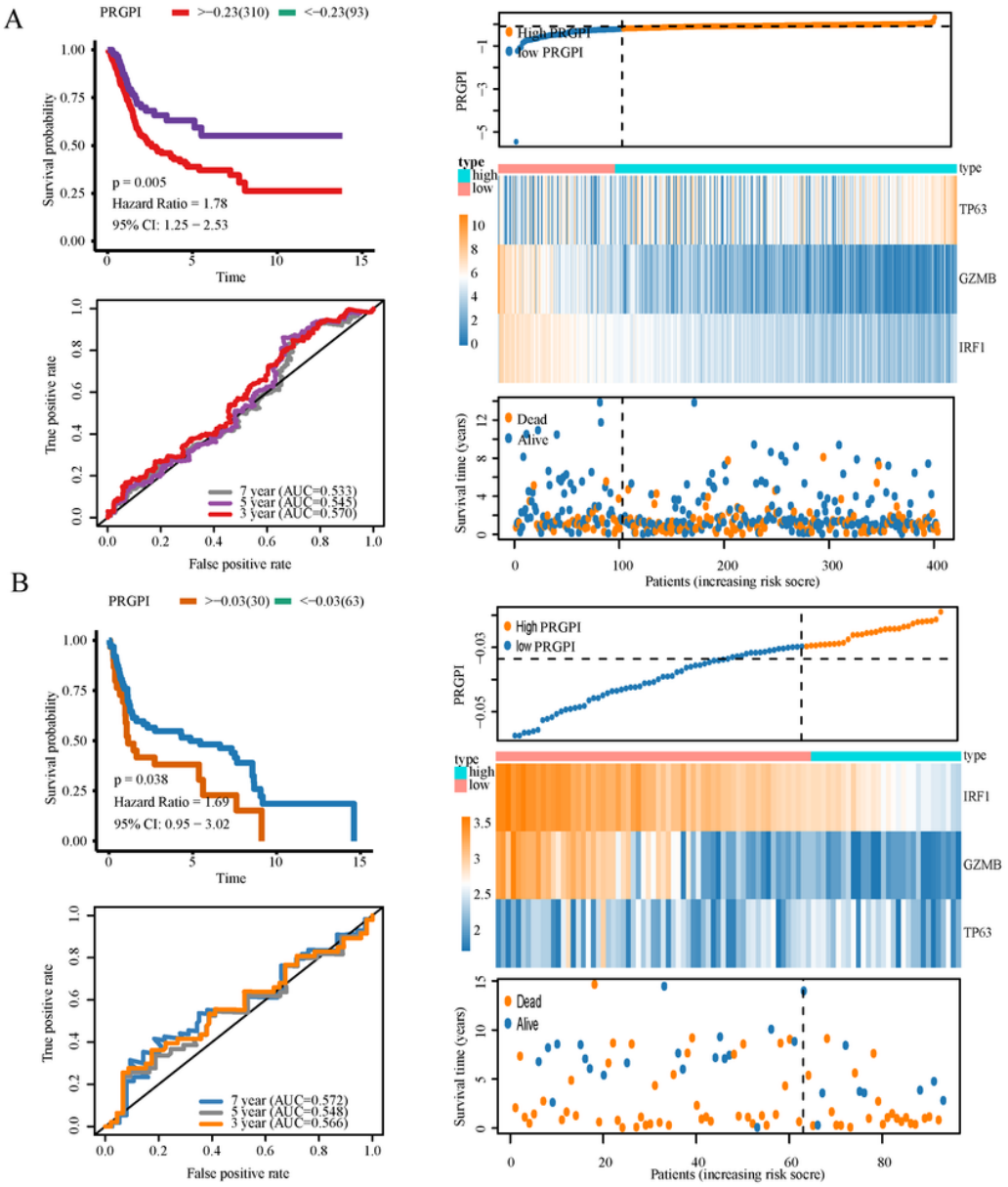

Figure 5

The prognostic significance of PRGPI in the cohort TCGA-BLCA and GSE31684. (A) KM analysis, ROC curve, and distribution heat map of TCGA-BLCA. (B) GSE31684.

Figure 6

Build the nomogram in the IMvigor210 cohort. (A) Nomogram diagram. (B) Calibration curve. (C) ROC curve.

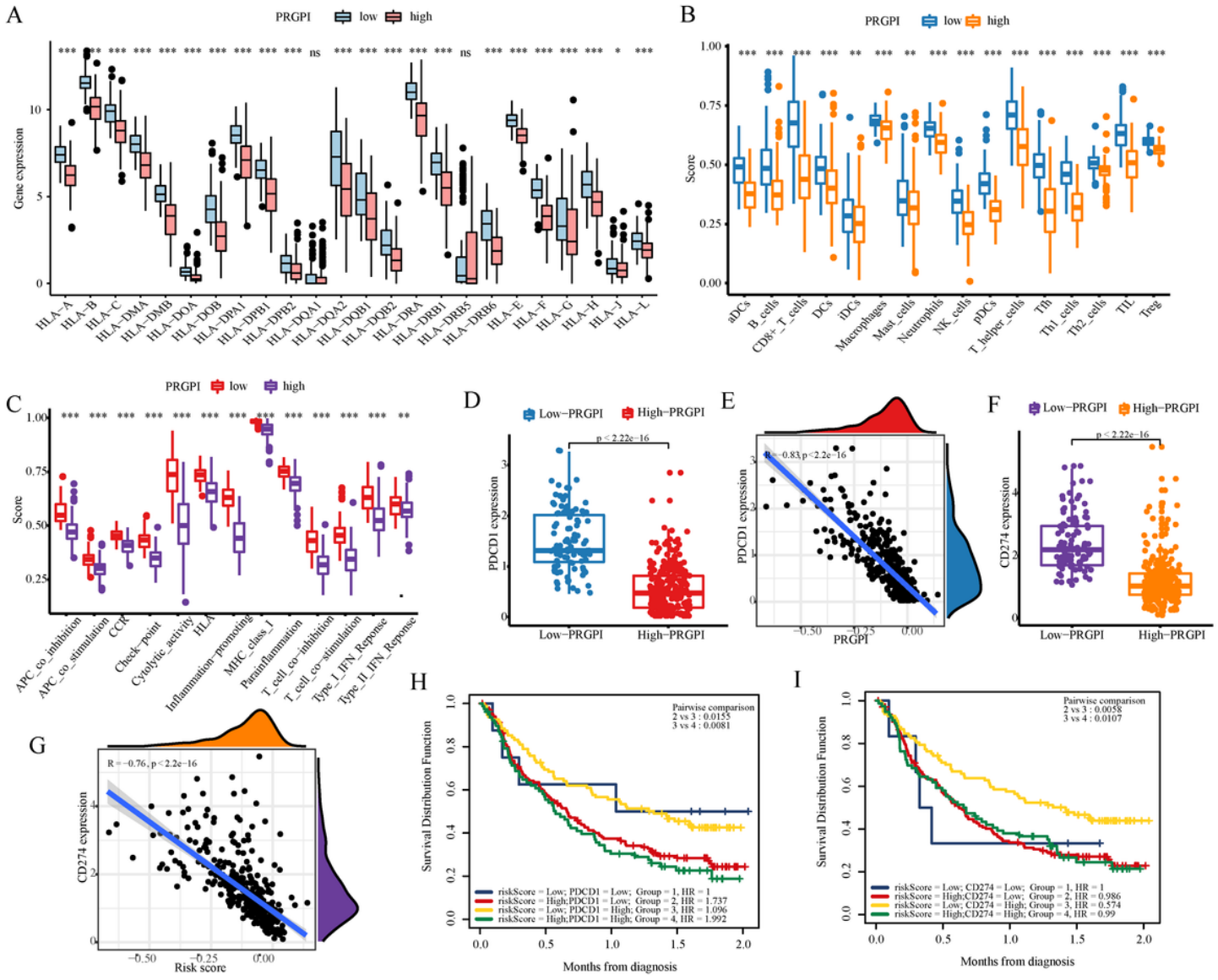

Figure 7

Analysis of PRGPI and immune characteristics based on IMvigor210 cohort. (A) The differential expression of HLA molecules in H-PRGPI and L-PRGPI groups. (B) Immune cells. (C) Immune-related

pathways. (D) The differential expression of PDCD1. (E) Co-expression analysis of PDCD1 and PRGPI. (F) The differential expression of CD274. (G) Co-expression analysis of CD274 and PRGPI (H) Joint survival analysis of PDCD1 and PRGPI. (I) Joint survival analysis of CD274 and PRGPI.

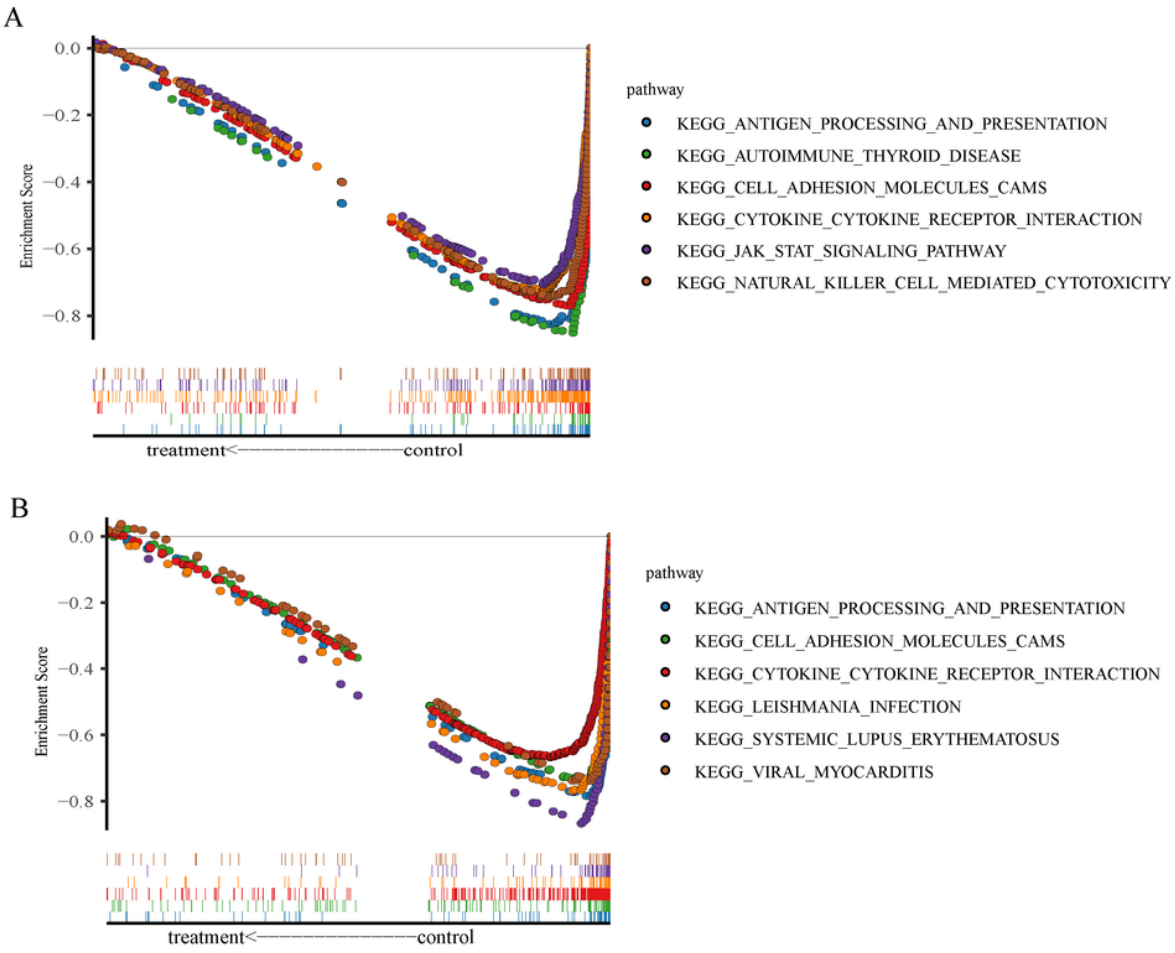

Figure 8

Gene set enrichment analysis. (A) IMvigor210 cohort. (B) GSE176307.

Supplementary Files

This is a list of supplementary files associated with this preprint. Click to download.

- Supplementaryfigure1.tif
- Supplementaryfigure2.tif
- Supplementaryfigure3.tif
- Supplementaryfigure4.tif